The effect of wind shear and curvature on orographic gravity wave drag produced by a mountain ridge

Miguel A. C. Teixeira and Pedro M. A. Miranda

Centro de Geofísica and Department of Physics,

University of Lisbon, Lisbon, Portugal

Submitted to the *Journal of the Atmospheric Sciences*

Submitted 7 January 2004

Corresponding author address:

Miguel A. C. Teixeira

Centro de Geofísica da Universidade de Lisboa,

Edifício C8, Campo Grande, 1749-016 Lisbon, Portugal

Tel: +351 21 7500884, Fax: +351 21 7500977

e-mail: mateixeira@fc.ul.pt

ABSTRACT

The analytical model proposed by Teixeira, Miranda & Valente is modified to calculate the gravity wave drag exerted by a stratified flow over a 2D mountain ridge. The drag is found to be more strongly affected by the vertical variation of the background velocity than for an axisymmetric mountain. In the hydrostatic approximation, the corrections to the drag due to this effect, as well as the perturbed quantities of the flow at the surface, including the pressure, may be calculated analytically.

1. Introduction

Recently, Teixeira et al. (2004) presented a linear model of mountain waves for wind profiles with shear and curvature, based on the WKB approximation. This model provided new analytical expressions for the wave drag as a function of the first and second derivatives of the background velocity profile. These expressions were shown to be asymptotically in agreement with previously known exact formulae, and to reproduce to a good degree of approximation the results of numerical mesoscale simulations, for similar input conditions. They were able to elucidate, in particular, why two flows that turn with height in different ways lead to opposite dependencies of the drag on the Richardson number.

Teixeira et al. (2004) considered the drag of hydrostatic flow over an isolated axisymmetric mountain. Two-dimensional (2D) orography is also frequently used in idealized studies of mountain waves, since it roughly approximates elongated ridges, which are common in nature. It is therefore of great practical interest to study the drag on this type of orography, for which the equations of motion simplify considerably due to the symmetry. In this note, the model of Teixeira et al. (2004) is extended to calculate the gravity wave drag associated with hydrostatic flow over an isolated 2D ridge.

The property that the corrections to the drag due to the variation of the wind with height are independent of the detailed shape of the orography is shown to hold also in the present case. However, the coefficients of these corrections are different from the axisymmetric case, due to the different geometry of the problem. Furthermore, in the case of a bell-shaped ridge (and presumably also for other simple types of orography), the perturbations of the flow variables at the surface may be calculated analytically.

2. Model equations

Consider stably stratified flow over an infinite isolated 2D mountain ridge. If a reference frame is defined such that the ridge is aligned in the y direction, and the background state of the atmosphere is horizontally uniform, the perturbations associated with the internal gravity waves generated by this orography are independent of y. If the fundamental equations of motion with the Boussinesq approximation are linearized with respect to these perturbations (which can be done if they are sufficiently small), and the perturbations are expressed as Fourier integrals along x, an equation may be derived for the vertical structure of $\hat{w}$, the Fourier transform of the vertical velocity perturbation:

$$\hat{w}'' + \left(\frac{N^2}{U^2} - \frac{U''}{U} \right) \hat{w} = 0. \tag{1}$$

Here N is the Brunt-Väisälä frequency (assumed constant), U is the background velocity (along x) and the primes denote differentiation along the vertical direction, z. This equation was obtained assuming additionally that the flow is steady and hydrostatic. Compared with eq. (13) of Teixeira et al. (2004), (1) is simplified by the symmetry along y, which means that the y component of the horizontal wavenumber vector $\mathbf{k} = (k_1, k_2)$ is $k_2 = 0$. For that reason, the horizontal wavenumber will be called simply k.

As is well known, when the coefficient multiplying $\hat{w}$ in (1) varies relatively slowly with z, this equation may be solved using the WKB approximation. Following Teixeira et al. (2004), the approximate WKB solution of (1) valid up to second order in the small perturbation parameter, ε, is

$$\hat{w} = \hat{w}(z=0) \exp \left\{ i \int_0^z \left(m_0(\varepsilon z') + \varepsilon m_1(\varepsilon z') + \varepsilon^2 m_2(\varepsilon z') \right) dz' \right\}, \tag{2}$$

where m_0, m_1 and m_2 are the zeroth, first and second-order coefficients of the series expansion of the vertical wavenumber of the internal gravity waves in powers of ε.

When introduced into (1), the solution (2) yields the following definitions:

$$m_0 = \frac{N}{U}\text{sign}(k), \tag{3}$$

$$\varepsilon m_1 = -\frac{i}{2}\frac{U'}{U}, \tag{4}$$

$$\varepsilon^2 m_2 = -\frac{1}{8}\frac{U}{N}\text{sign}(k)\left(\frac{U'^2}{U^2} + 2\frac{U''}{U}\right). \tag{5}$$

In (3)-(5), the radiation boundary condition at $z \to +\infty$ is implicitly assumed, since the sign of m_0 and m_2 is the same as that of k, implying upward energy propagation. These expressions are analogous to eqs. (22)-(24) of Teixeira et al. (2004), but simplified for 2D, hydrostatic flow. With the addition of the boundary condition at the surface

$$\hat{w}(z=0) = iU_0 k\hat{\eta}, \tag{6}$$

the solution to the problem is fully specified. Here $\hat{\eta}$ is the Fourier transform of the surface elevation and the subscript 0 applied to the background velocity denotes its value at the surface.

3. **Mountain wave drag**

For a 2D mountain ridge, the total gravity wave drag is infinite, and it only makes sense to define a drag per unit length in the transverse direction. In the linear approximation, this is given by

$$D = \int_{-\infty}^{+\infty} p(z=0)\frac{\partial \eta}{\partial x}dx, \tag{7}$$

where p is the pressure and η is the surface elevation. The drag can also be calculated in Fourier space, through the integral

$$D = 2\pi i \int_{-\infty}^{+\infty} k\hat{p}^*(z=0)\hat{\eta}dk, \tag{8}$$

where k is the wavenumber (along x) and $\hat{p}^*$ is the complex conjugate of the Fourier transform of the pressure.

$\hat{p}(z=0)$ is given, in the present approximation, by

$$\hat{p}(z=0) = i\rho_0 U_0^2 \left(m_0(z=0) + \varepsilon m_1(z=0) + i\frac{U_0'}{U_0} + \varepsilon^2 m_2(z=0) \right) \hat{\eta}, \tag{9}$$

where ρ_0 is the reference density of air (cf. eq. (31) of Teixeira et al. 2004). Using the results (3)-(5), (9) becomes

$$\hat{p}(z=0) = i\rho_0 N U_0 \left[\mathrm{sign}(k) + \frac{i}{2}\frac{U_0'}{N} - \frac{1}{8}\mathrm{sign}(k) \left(\frac{U_0'^2}{N^2} + 2\frac{U_0 U_0''}{N^2} \right) \right] \hat{\eta}. \tag{10}$$

Introducing the complex conjugate of this equation into (8), the drag may be written

$$D = 2\pi\rho_0 N U_0 \left(1 - \frac{1}{8}\frac{U_0'^2}{N^2} - \frac{1}{4}\frac{U_0 U_0''}{N^2} \right) \int_{-\infty}^{+\infty} |k||\hat{\eta}|^2 dk. \tag{11}$$

In (11), $|k|$ appears inside the integral because of the sign(k) factor in the terms of zeroth and second order in ε of the pressure perturbation, $\hat{p}$. The part of the drag corresponding to the first-order term cancels, because the sign(k) factor is absent. Since $|\hat{\eta}|^2$ is even when the surface elevation function $\eta(x)$ is real, this part of the integral is zero, because the corresponding integrand is odd.

Noting that, by (11), the drag in the absence of shear is defined as

$$D_0 = 2\pi\rho_0 N U_0 \int_{-\infty}^{+\infty} |k||\hat{\eta}|^2 dk, \tag{12}$$

the drag for the general case may be expressed more compactly as

$$D = D_0 \left(1 - \frac{1}{8}\frac{U_0'^2}{N^2} - \frac{1}{4}\frac{U_0 U_0''}{N^2}\right), \tag{13}$$

and it is clear that the corrections to the drag due to shear and curvature of the background wind profile do not depend on the form of the function $\hat{\eta}$. This equation, which is analogous to eqs. (50)-(51) of Teixeira et al. (2004), is nevertheless much shorter, due to the simplifications brought by the 2D geometry.

The drag given by (13) is per unit length and so cannot be directly compared with the drag calculated by Teixeira et al. (2004), but the relative corrections due to the shear and curvature of the wind profile, put in evidence by (13), are of a similar nature and may be compared. These corrections differ from those valid for an axisymmetric mountain, with the 1/8 and 1/4 coefficients, multiplying respectively $U_0'^2/N^2$ and $U_0 U_0''/N^2$ in (13), being larger by a factor of 4/3. This means that the effect on the drag of the shear and curvature of the wind profile is qualitatively similar, but stronger for 2D than for 3D flow.

For a linear wind profile of the form

$$U = U_0 \left(1 - \frac{z}{z_c}\right), \tag{14}$$

where z_c is constant, (13) reduces to

$$D = D_0 \left(1 - \frac{1}{8\mathrm{Ri}}\right), \tag{15}$$

where $\mathrm{Ri} = N^2/U_0'^2 = N^2 z_c^2/U_0^2$ is the Richardson number of the flow. This expression may be compared with the corresponding result obtained analytically by Smith (1986) for a linear profile with an arbitrarily large shear rate. It may be shown that, in the present notation, Smith's drag expression (his eq. (3.17)) is

$$D = D_0 \left(1 - \frac{1}{4\mathrm{Ri}}\right)^{1/2}, \tag{16}$$

and it is straightforward to show that both expressions are asymptotically equal in the limit of large Ri. The consistency of the two approaches, which parallels the asymptotic agreement found between the 3D model of Teixeira et al. (2004) and the exact drag expression of Grubišić & Smolarkiewicz (1997), gives further confidence in the WKB approach adopted here.

Figure 1a shows a comparison between the normalized drag given by (15) and data taken from the mesoscale, non-hydrostatic numerical model NH3D (Miranda & James 1992). This model is 3D, but is run here for a 2D ridge using a sufficiently wide domain of integration. The conditions considered in the runs were very approximately linear and hydrostatic, in order to isolate the effect of shear. Also shown is the drag given by Smith's expression, (16). It may be seen that the agreement with (15) is nearly as good as with (16). However, the value taken by D/D_0 at $\mathrm{Ri} = 1/4$ is larger than zero, in contradiction with what is predicted by (16). Since for this value of Ri, the flow should be close to becoming unstable, neither analytical result is formally accurate.

When the wind profile is more complicated than (14), both shear and curvature terms are important in (13). An early attempt to evaluate the effect of the curvature of the wind profile on the surface drag on a 2D ridge using a WKB approximation was made by Grisogono (1994). In the present notation, and for inviscid conditions, Grisogono's drag expression (his eq. (4.8)) reads

$$D = D_0 \left(1 - \frac{1}{2} \frac{U_0 U_0''}{N^2} \right). \tag{17}$$

The coefficient multiplying the curvature term is larger by a factor of 2 than that present in (13) and the term proportional to $U_0'^2$ is absent. The reasons for these discrepancies have to do with an inconsistent application of the WKB method and are discussed in detail by Teixeira et al. (2004).

When studying the effect of curvature of the wind profile on mountain wave drag in 2D, it is not possible to consider a flow simultaneously with constant N and constant Richardson number, as was done for the 3D situation by Teixeira et al. (2004). So, the simplest flow with non-zero second derivative, a parabolic wind profile, is considered next:

$$U = U_0 \left[1 - \left(\frac{z}{z_c} \right)^2 \right]. \tag{18}$$

In this flow $U_0' = 0$, hence the Richardson number at the surface is infinite. However, the curvature is $U_0'' = -2U_0/z_c^2$, and this can be related to the Richardson number at the critical level ($z = z_c$), $\mathrm{Ri}_c = N^2 z_c^2 / 4U_0^2$, which is the important parameter for this flow. It turns out that the drag expression (13) reduces in this case to

$$D = D_0 \left(1 + \frac{1}{8\mathrm{Ri}_c} \right). \tag{19}$$

So, the drag increases as Ri_c decreases, unlike the previous case, despite the qualitative similarity of the background wind profiles (14) and (18).

In figure 1b, the drag calculated with (19) is compared with data from numerical simulations of the NH3D model for approximately linear and hydrostatic conditions. Also shown is the prediction from Grisogono's formula, (17). It is clear that the prediction of (19) is not as good as in the previous case, with some drag underestimation, especially at relatively low Ri_c. This resembles the behavior of the drag for a turning wind over an axisymmetric mountain in figure 7 of Teixeira et al. (2004), where the curvature is also negative at the surface. Nevertheless, qualitatively, and in order-of-magnitude terms, the agreement is satisfactory. Curiously, (17) gives a better prediction of the drag than expected due to this behavior, but is clearly inferior to (19), especially for large Ri_c.

4. **The surface pressure perturbation**

In order to understand the behavior of the drag, it is useful to calculate the surface pressure perturbation (as was done in 3D by Teixeira et al. 2004). In fact, at the surface, it is straightforward to calculate, not only the pressure, but also all other relevant variables of the flow. However, some of them, such as the vertical velocity perturbation, the buoyancy perturbation, b, and the spanwise velocity perturbation, v, are related in a trivial way to the surface elevation, η. Apart from the pressure, the only other variable of the flow that is affected at the surface by the vertical variation of the background velocity is the streamwise velocity perturbation, u (which is relevant for downslope windstorms).

$p(z = 0)$ may be obtained by calculating the inverse Fourier transform of (10).

Although the only expressions depending on k in (10) are sign(k) and $\hat{\eta}$, and this renders the integration analytical in most cases, the presence of sign(k) means that $\hat{\eta}$ must be specified. Here, an isolated bell-shaped ridge will be used as an example. The corresponding Fourier transform is

$$\hat{\eta} = \frac{1}{2} h a \mathrm{e}^{-a|k|}, \tag{20}$$

where h is the maximum elevation and a is the half-width of the ridge.

Then, it is found from (10) that

$$\frac{p(z=0)}{\rho_0 N U_0 h} = -\left(1 - \frac{1}{8}\frac{U_0'^2}{N^2} - \frac{1}{4}\frac{U_0 U_0''}{N^2}\right)\frac{x/a}{1+(x/a)^2} - \frac{1}{2}\frac{U_0'}{N}\frac{1}{1+(x/a)^2}. \tag{21}$$

The pressure perturbation thus comprises two parts: the first one, which is anti-symmetric with respect to the ridge, produces drag; the second one, which is symmmetric, and in fact proportional to the surface elevation, does not produce drag.

Figure 2a shows the pressure perturbation as a function of streamwise distance for different values of Ri, for the linear background velocity profile (14). The continuous lines correspond to expression (21), while the symbols represent output from the NH3D numerical model. For high Ri, the pressure distribution tends to be anti-symmetric with respect to the orography, in agreement with the linear theory of Smith (1980). As Ri decreases, the anti-symmetric component of the pressure perturbation weakens and the symmetric component becomes more prominent. The analytical expression reproduces the numerical simulation data quite accurately, except for Ri = 0.25, confirming that the WKB approximation can be used for Ri as low as 0.5 (as happened in the 3D case). Of course, this is also consistent with the behavior of the drag in figure 1a.

Figure 2b presents the pressure perturbation for the parabolic background velocity profile (18). In this case $U_0' = 0$, and hence, according to (21), the symmetric component of the pressure vanishes. The pressure perturbation is thus predicted to be perfectly anti-symmetric. When the analytical results given by (21) are compared with the numerical results, this aspect is confirmed, except for $\mathrm{Ri}_c = 0.25$, and to a much lesser degree for $\mathrm{Ri}_c = 0.5$. However, the magnitude of the pressure is considerably underestimated by the analytical model for $\mathrm{Ri}_c > 1$. This is consistent with the worse prediction of the drag, when compared with the previous case, for similar values of Ri.

Especially for the linear background velocity profile, the pressure perturbation given by the NH3D model tended to drift slightly in time, so as to appear in the plots translated vertically upward or downward by a constant when compared with the analytical result, although its shape was in close agreement. This feature, which is related to imperfections in the implementation of the boundary conditions in the numerical model, has been corrected by subtracting from the pressure perturbation given by NH3D the integral of the pressure over the domain,

$$\int_{-L}^{L} \frac{p(z=0)}{\rho_0 N U_0 h} dx, \tag{22}$$

and adding to it the theoretical value of this integral, which from (21) is seen to be

$$\int_{-L}^{L} \frac{p(z=0)}{\rho_0 N U_0 h} dx = -\frac{U_0'}{N} \arctan\left(\frac{L}{a}\right) = -\mathrm{sign}(U_0')\mathrm{Ri}^{-1/2} \arctan\left(\frac{L}{a}\right). \tag{23}$$

In (22) and (23), L is the half width of the domain. Obviously, in these expressions, only the symmetric part of the pressure contributes to the integral of the pressure perturbation so, for the parabolic velocity profile, the integral is zero.

5. Discussion

The calculations carried out in this study are relevant for the parameterization of gravity wave drag in flow over elongated ridges. As for an axisymmetric mountain, it appears that the drag depends, to a first approximation, on the characteristics of the background flow at the surface, at least for linear and hydrostatic conditions. The slightly worse performance of the model for the velocity profile with curvature, caused undoubtedly by the variation with height of the background velocity gradient, does not contradict this conclusion.

The effects of shear and curvature of the wind profile are qualitatively similar to those for flow over an axisymmetric mountain (with negative curvature increasing the drag and shear decreasing it), but stronger. This probably happens because a larger fraction of the air becomes affected by the background velocity gradient, as it is forced to flow over the ridge, instead of being able to flow around the mountain. For related reasons, it is necessary to be cautious when extrapolating these results to large amplitude ridges: nonlinear effects are known to be more important in 2D than in 3D geometries (Miranda & James 1992).

Apart from its intrinsic scientific interest and practical relevance, mountain wave drag in flow over ridges is also amenable to much more detailed comparisons with numerical simulations. Due to the simplified geometry, the resolutions used in these simulations can be much higher than in 3D simulations.

Acknowledgments. This work was supported by Fundação para a Ciência e Tecnologia (FCT) under grant SFRH/BPD/3533/2000 and project BULET/33980/99, cofinanced by the European Union under program FEDER.

REFERENCES

Grisogono, B., 1994: Dissipation of wave drag in the atmospheric boundary layer. *J. Atmos. Sci.*, **51**, 1237–1243.

Grubišić, V. and P. K. Smolarkiewicz, 1997: The effect of critical levels on 3D orographic flows: linear regime. *J. Atmos. Sci.*, **54**, 1943–1960.

Miranda, P. M. A. and I. N. James, 1992: Non-linear three dimensional effects on the wave drag: splitting flow and breaking waves. *Quart. J. Roy. Meteor. Soc.*, **118**, 1057–1081.

Smith, R. B., 1980: Linear theory of stratified hydrostatic flow past an isolated obstacle. *Tellus*, **32**, 348–364.

Smith, R. B., 1986: Further development of a theory of lee cyclogenesis. *J. Atmos. Sci.*, **43**, 1582–1602.

Teixeira, M. A. C., P. M. A. Miranda and M. A. Valente, 2004: An analytical model of mountain wave drag for wind profiles with shear and curvature. *J. Atmos. Sci.*, in press.

Figure Captions

Figure 1 Normalized drag as a function of the inverse Richardson number. (a) Linear background velocity profile, (14). (b) Parabolic background velocity profile, (18). The NH3D model uses $Na/U_0 = 23$, $Nh/U_0 = 0.01$.

Figure 2 Normalized pressure perturbation at $z = 0$ as a function of normalized streamwise distance. (a) Linear background velocity profile, (14). (b) Parabolic background velocity profile, (18). Analytic results are calculated from (21).

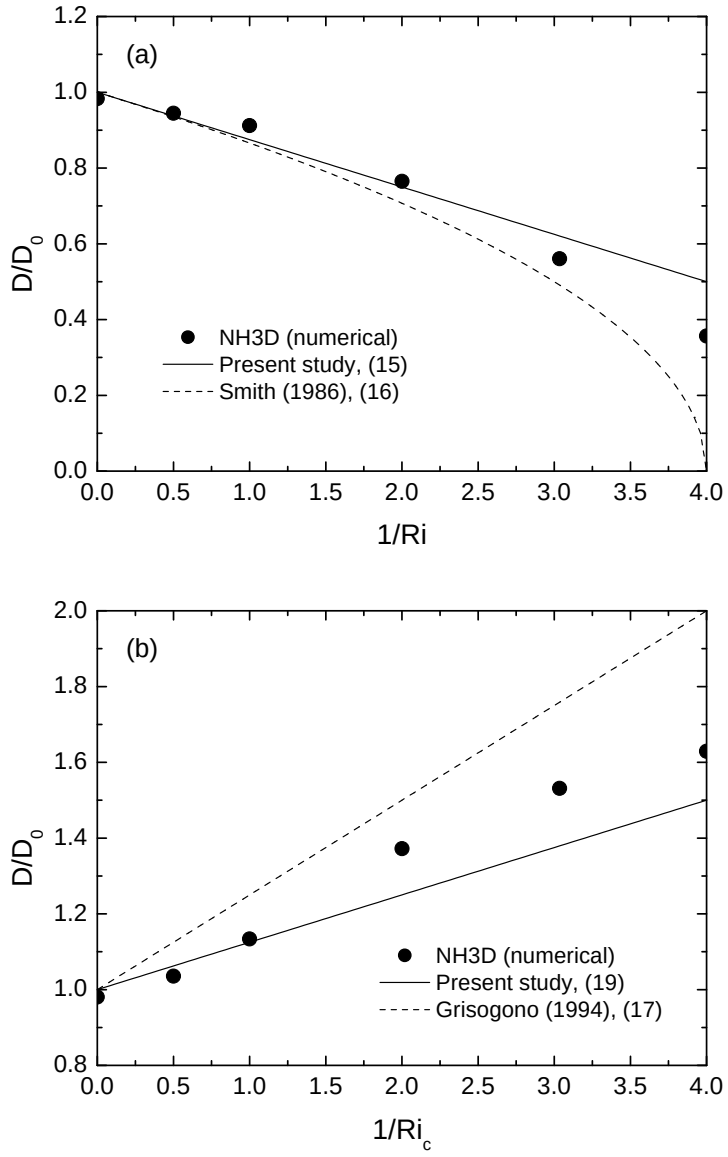

Figure 1: Normalized drag as a function of the inverse Richardson number. (a) Linear background velocity profile, (14). (b) Parabolic background velocity profile, (18). The NH3D model uses $Na/U_0 = 23$, $Nh/U_0 = 0.01$.

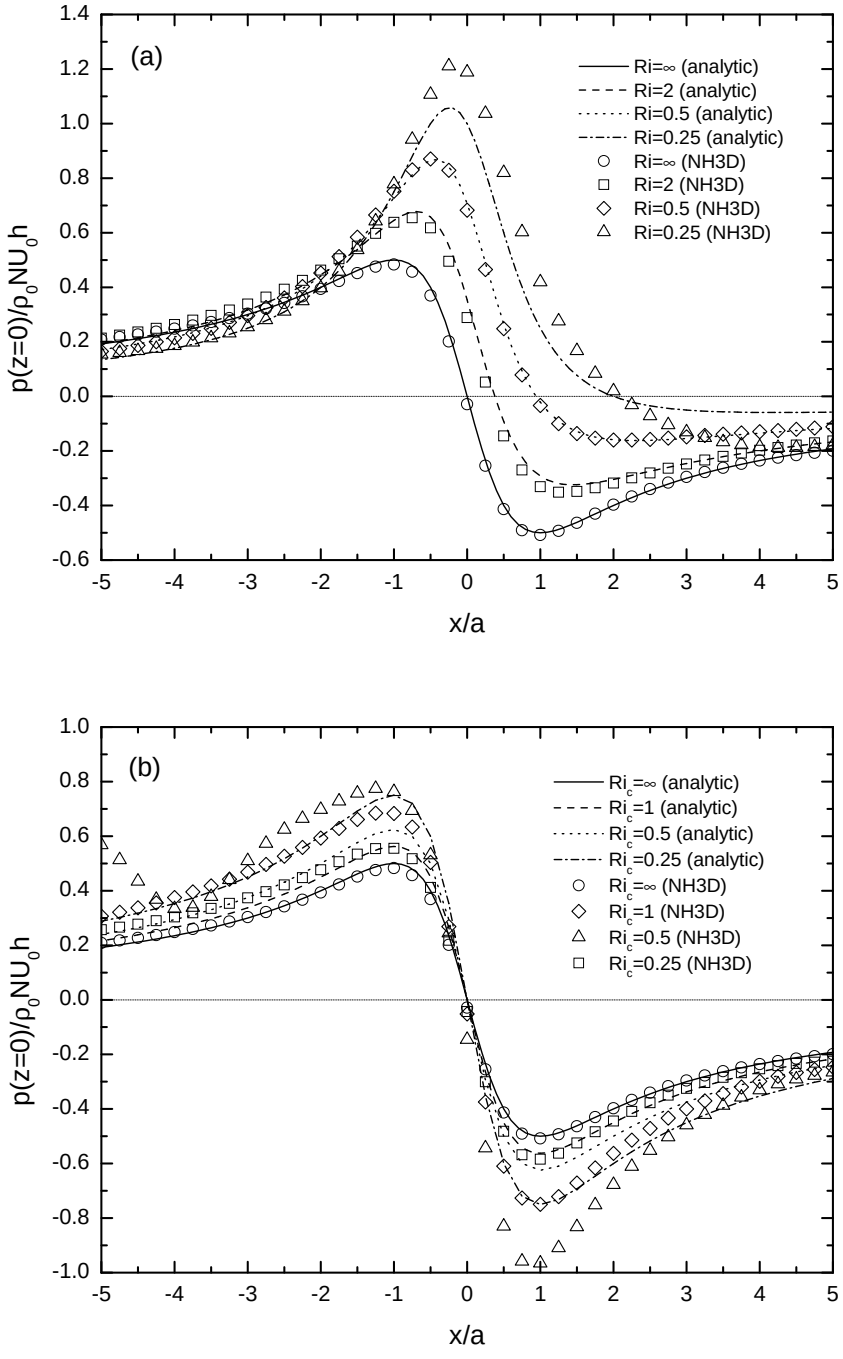

Figure 2: Normalized pressure perturbation at $z = 0$ as a function of normalized streamwise distance. (a) Linear background velocity profile, (14). (b) Parabolic background velocity profile, (18). Analytic results are calculated from (21).